

Optical Properties of Spin-Deposited Nanocrystalline Ni-Zn Ferrite Thin Films Processed by Sol-Gel

C. S. Pawar¹ · M. P. Gujar² · V. L. Mathe³

Received: 24 July 2016 / Accepted: 13 August 2016 / Published online: 11 October 2016
© Springer Science+Business Media New York 2016

Abstract Nano crystalline Zn-substituted Ni ferrite films with compositions of $\text{Ni}_{1-x}\text{Zn}_x\text{Fe}_2\text{O}_4$ ($x = 0.25, 0.50, 0.75$) were synthesized by sol-gel spin coating method. The synthesized films were characterized for their structural, morphology, optical, electric, and magnetic properties using x-ray diffraction, scanning electron microscope, UV-Vis spectrometer, two probe resistivity, and vibrating sample magnetometer techniques, respectively. The corresponding results indicate that zinc content has significant effect on physical, magnetic, and optical properties of the ferrite. X-ray diffraction studies of thin films showed that the samples have pure cubic spinel phase. The crystallite size is of the nanoparticles estimated using Debye-Scherrer's method was found to be in the range of 10.27 to 14.97 nm. The lattice parameter was found to be increased from 8.35 to 8.40 Å with increasing Zn^{2+} contents. The morphology of the thin films depicted the formation of well-developed nano-sized clusters with homogeneous and agglomerated. The optical absorption seen to be affected due to the presence of Zn in Ni-Zn ferrite thin films. Ni-Zn ferrite thin films possess small coercivity and remnant magnetization, which indicates the soft magnetic nature of the material. Electrical

resistivity of the films decreases with increasing temperature, suggesting the semiconducting nature of the samples.

Keywords Ni-Zn ferrite films · Sol-gel spin coating · Optical properties

1 Introduction

Thin films of AB_2O_4 -type spinel ferrite having interesting magnetic properties are considered as potential candidate than that of their same bulk form, due to their tunable structural, optical, morphological, magnetic, electrical, and catalytic properties [1–6]. Among spinel ferrite, nickel zinc ferrite is the most popular composition of soft ferrite. It is used in electronic devices because it has the soft ferrites with low power loss and high permeability. Due to low eddy current losses and coercivity and high resistivity, Ni-Zn ferrite has high-frequency applications such as a core material for power transformer, circuit inductors in the megahertz frequency region. Properties of ferrites are found to be highly sensitive to their microstructure and chemical composition. Zinc content in Ni-Zn ferrite plays an important role for determination of the properties of ferrites. Ni-Zn ferrites are magnetic materials of immense technological importance with diverse applications such as high and low frequency transformer cores, microwave devices, and antenna rods [7].

In case of $\text{Ni}_{1-x}\text{Zn}_x\text{Fe}_2\text{O}_4$ spinel ferrite system, NiFe_2O_4 forms inverse, ZnFe_2O_4 forms the normal, but Ni-Zn forms a mixed spinel structure. Spinel ferrites are important technological materials due to their semiconducting and ferrimagnetic properties [7]. The possible applications of the ferrite nanoparticles are in magnetic storage, magnetic

✉ C. S. Pawar
charudutta_p@yahoo.com

¹ Material Science and Thin Film Research Laboratory,
Department of Physics, Shankarrao Mohite Mahavidyalaya,
Akluj, India

² Shri. Shivaji Junior College, Bawada, Pune, India

³ Department of Physics, Savitribai Phule Pune University,
Pune 411 007 India

guided drug delivery agents, and gas sensors [8, 9]. Ferrite nanoparticles having band gap of ~ 2 eV offer several advantages including visible light absorption, magnetic separability, and enhanced photocatalytic efficiency due to the presence of extra catalytic sites in their crystal structures [10]. The electrical and magnetic properties of the materials depend on its micro structural properties which are related to its method of preparation. Ni-Zn is more stable than the other types of ferrites, easily manufactured, low cost, and has excellent and desirable magnetic properties.

For several decades, Ni-Zn ferrite is prepared by conventional ceramic method, which requires high temperature to complete the solid state reaction. The high temperature also leads to zinc loss during the annealing process.

Recently, trend for downloading of electronic equipments in general and potential applications of Ni-Zn ferrite components in planar microwave magnetic devices have necessitated the fabrication of ferrites in the form of thin films. Ni-Zn ferrite thin films may play an important role in facilitating the design and fabrication of devices such as micro-inductors, micro-transformers, and microwave non-reciprocal devices [11]. In the literature, there are numerous reports on the fabrication of ferrite thin films using various techniques such as sol-gel [12], spin spray ferrite plating [13], sputtering [14], pulse laser deposition [15], citrate precursor [16], and spin spray [17], etc. Recently, the sol-gel spin coating technique has received enormous attention because of its simplicity, affordable instrumentations, low cost, and controllable growth temperatures [18]. Javed Alam Khan et al. reported synthesis of polyaniline/CoFe₂O₄ nano composites using in situ polymerization method investigated their influence on optical properties. Also, photo-catalytic activity of synthesized nano composites was measured [19]. Mohd Qasim et al. synthesized Ni_{0.5}Zn_{0.5}Fe₂O₄/Zn_{0.95}Ni_{0.05}O by egg albumen-assisted sol-gel techniques and studied its optical and photo-catalytic properties [20].

The electrical and magnetic properties of the ferrites have been mostly investigated because of its wide spread in electrical and electronic devices. Optical properties, however, have been relatively rarely studied.

Optical tests giving transmittance and absorbance spectra used to determine optical constants such as refractive index, extinction coefficient, and dielectric constants [21, 22]. Optical absorption spectra provide the necessary parameters to determine direct and indirect transitions in the band gaps of the materials [23]. In a semiconductor material band gap is the difference between the conduction and valance band potentials. Optical properties may affect the microstructure of the film, grain size, and the processing technique. In practice, the optical properties of a material are of considerable importance for integrated applications directly with optic devices as filters, modulators, and switches.

Here, we report synthesis of Ni-Zn ferrite thin films using sol-gel spin coating techniques, which is known for its simplicity, low cost, produces uniform thin layer, and productive technique. This paper aims to synthesize and to elucidate optical, electrical, and magnetic properties sol-gel synthesized Ni-Zn thin films.

2 Experimental

2.1 Synthesis

All the ingredients used to obtain Ni-Zn ferrite thin films were analytical grade which were used without further purification or treatment. The chemical reagents used in this work Zn(CH₃COO)₂·2H₂O, Ni(CH₃COO)₂·4H₂O, and Fe(NO₃)₃·9H₂O in stoichiometric quantities. The flowchart used to obtain the Ni-Zn thin films is shown in Fig. 1. The procedure to obtain thin films is similar to that reported by us for Ni_{0.25}Zn_{0.75}Fe₂O₄ film [24]. Two methoxy ethanol was used for preparation of all samples. Similar method is used for the synthesis of Ni_{1-x}Zn_xFe₂O₄ ($x = 0.25, 0.5$). The films were annealed at 450 °C for 12-h. The films so obtained show good adhesion with the substrate.

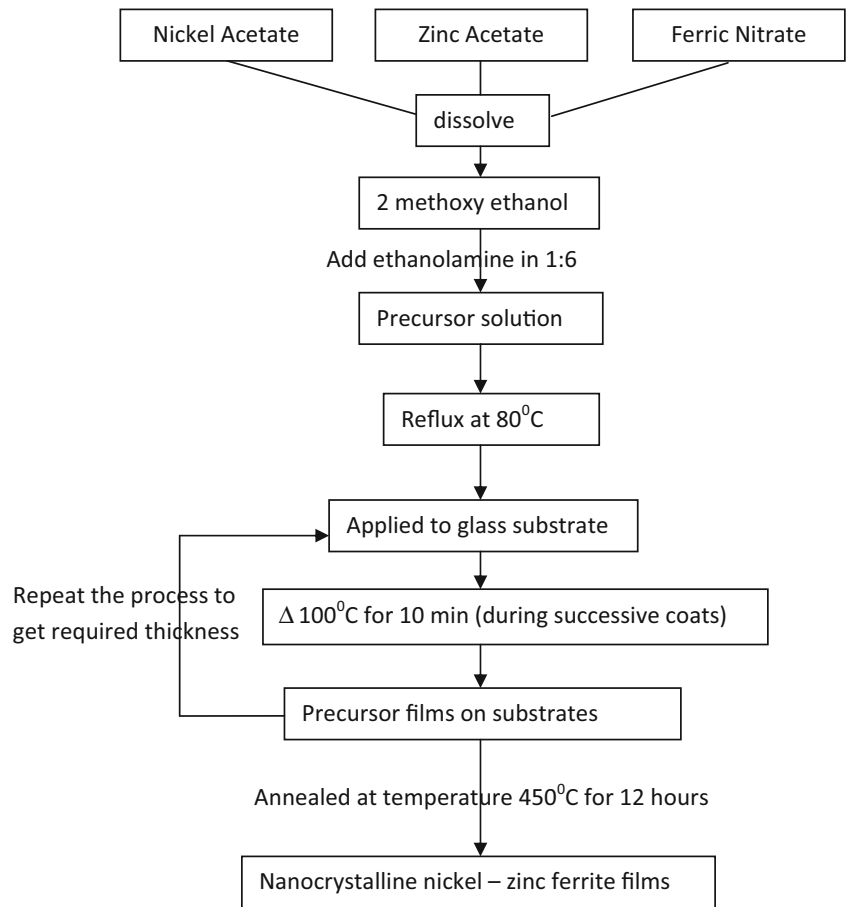
The films were characterized by x-ray diffractometer (model Bruker D8 Advance) (XRD) using Cu-K α radiation for the confirmation of phase and structure. The SEM micrographs of the synthesized films were recorded using scanning electron microscope (model JEOL JSM 6360). Optical properties were recorded using UV-VIS-NIR spectrophotometer Systronics-119 in the wavelength range 200–800 nm. High-purity silver paint was applied on the surface of thin film for ohmic contacts. The DC resistivity (ρ_{DC}) measurements of zinc-doped nickel ferrite thin films were carried out using 2-probe method, where Tektronix make Digital Multimeter DMM 4050 was used to record the current at constant applied voltage of 5 V. DC resistivity measurements were carried out at and well above room temperature. Vibrating Sample Magnetometer Lakeshore Model 7307 was employed to record magnetic properties as a function of external magnetic field at room temperature.

3 Results and Discussion

3.1 Structural Characterization

XRD patterns of the Ni_{1-x}Zn_xFe₂O₄ ($x = 0.25, 0.5, 0.75$) ferrite films are shown in Fig. 2a–c. Well defined, intense diffraction peaks indicate that as-synthesized ferrite have good crystallinity. The diffraction lines observed at 30.2°, 35.5°, 43.1°, 53.4°, 56.9°, and 62.4° are assigned to (220), (311), (400), (422), (511), and (440) planes, respectively.

Fig. 1 Flow chart of Ni-Zn ferrite thin films



Presence of characteristics diffraction line around 35.5 indicates single-phase formation of spinel cubic phase without un-reacted or secondary phase. It was noted that crystallization of the films begins at temperatures below 500 °C. The

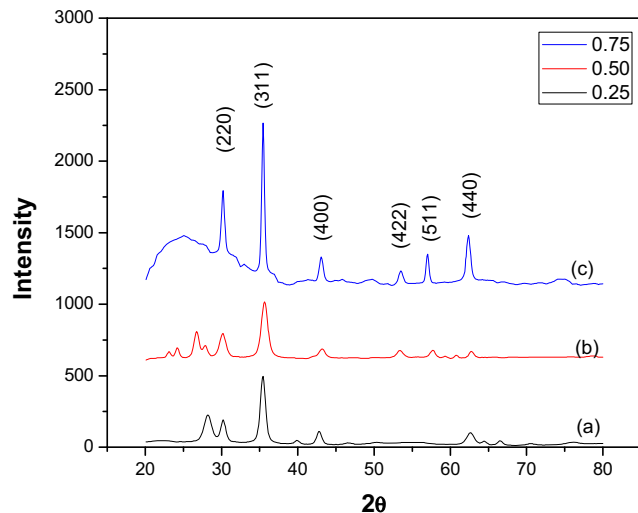


Fig. 2 XRD Spectra of **a** Ni_{0.75}Zn_{0.25}Fe₂O₄, **b** Ni_{0.5}Zn_{0.5}Fe₂O₄, **c** Ni_{0.25}Zn_{0.75}Fe₂O₄ ferrite thin film annealed at 450 °C for 12 h

characteristic peak (311) is prominent for all the samples under investigation.

The observed *d* values are in good agreement with JCPDS card 73-1960. The lattice constant *a* for all compositions was calculated from diffraction planes by using (1) and are listed in Table 1.

$$a = d\sqrt{h^2 + k^2 + l^2} \tag{1}$$

where *d* is the inter-planer spacing; *h*, *k*, and *l* are the miller indices of the crystal planes [25]. Increase in lattice constant leads to decreases in x-ray density. The theoretical densities

Table 1 Crystallite size, lattice constant, strain, and density of Ni_{1-x}Zn_xFe₂O₄ (*x* = 0.25, 0.5, 0.75) ferrite thin films

Zn content	Crystallite size nm	Lattice constant A°	Strain	Density (gm/cm ³)
0.25	10.27	8.35	0.0025	5.39
0.5	10.73	8.38	0.0042	5.35
0.75	14.97	8.40	0.0088	5.24

of the samples were calculated from the x-ray diffraction data using the relation (2) and are listed in Table 1.

$$\rho_x = \frac{8M}{Na^3} \quad (2)$$

where ρ_x is the density calculated from XRD data, M is the molecular weight, N is the Avogadro's constant ($6.022 \times 10^{23} \text{ mol}^{-1}$), and a is the lattice constant of the cubic unit cell [26].

From Table 1, it is noticed that the value of lattice constant slightly increases from 8.35 to 8.40 Å with the increase of Zn concentration. This result is comprehensively considered that the replacement of smaller Fe^{3+} ions with larger Zn^{2+} (0.74 Å) at tetrahedral sites. Thus, there is migration of smaller Fe^{3+} ions from tetrahedral to octahedral sites [27]. This expands the tetrahedral sites leading to an increase of the lattice constant [28]. The variation of lattice constant and density with Zn content are shown in Fig. 3.

The crystallite size (D) of each composition for annealed ferrite films was calculated from the full width at half-maximum (FWHM) of the strongest diffraction peak (311) using the Scherrer formula

$$D = \frac{0.9\lambda}{\beta \cos \theta} \quad (3)$$

where D is the crystallite size, λ is the wavelength of the x-ray source, β is the FWHM of the (311) diffraction peak, and θ is the position of diffraction angled. The value of crystallite size is listed in Table 1. It is also observed that as Zn content increases, there is increase in crystal size.

The grain size of ferrite films depends on different amounts of accumulated strain energy and neighboring grains; the grain growth is also mediated by neighboring grains that have different energies due to curvature

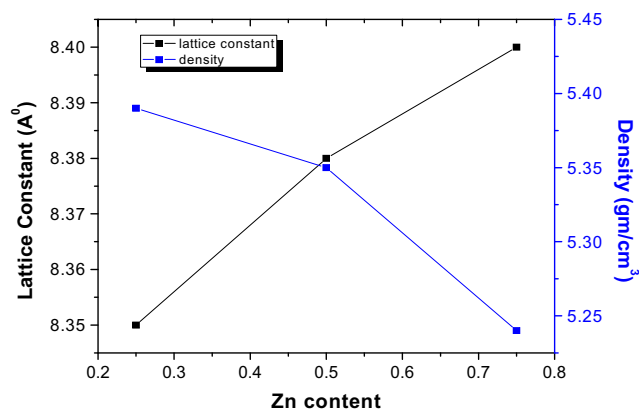


Fig. 3 Variation of lattice constant and density of $\text{Ni}_{1-x}\text{Zn}_x\text{Fe}_2\text{O}_4$ ($x = 0.25, 0.5, 0.75$) ferrite thin films

of energetic grain boundaries [29]. Strain ($\Delta d/d$) were calculated by using (4) [30]

$$\text{Strain} = \frac{\Delta d}{d} = \frac{d_{\text{exp}} - d_{\text{hkl}}}{d_{\text{hkl}}} \quad (4)$$

where d_{exp} is the experimental d spacing and d_{hkl} is d spacing taken from JCPDS card 73-1960. Strain in the film increases as Zn content increases.

The variation of crystallite size and strain with Zn content are shown in Fig. 4.

3.2 Scanning Electron Microscopy

The microphotographs of $\text{Ni}_{1-x}\text{Zn}_x\text{Fe}_2\text{O}_4$ ($x = 0.25, 0.5, 0.75$) ferrite films grown on glass substrate prepared using spin coating technique and annealed at 450° for 12 h are presented in Fig. 5a–c, respectively. From SEM, it is observed that the films are continuous and uniform without any crack. The grains are regular in shape and particles are found as agglomerated.

3.3 Optical Properties

Optical properties of Ni-Zn ferrite films were studied using optical absorption spectra recorded in the wavelength range of 200–800 nm. Absorbance spectra of $\text{Ni}_{1-x}\text{Zn}_x\text{Fe}_2\text{O}_4$ ($x = 0.25, 0.5, 0.75$) ferrite films grown on glass substrate using spin coating technique are presented in Fig. 6. It is seen from the graph that as wavelength increases, absorbance decreases in all cases. In all cases, absorbance is maximum at 400 nm. As we are increasing the Zn content, the absorbance goes on decreasing. It is seen that as the wavelength increases absorbance of the film decreases in a region 300 to 800 nm ranges. Figure 6 shows shift in absorption edge to low wavelength side with increase in Zn

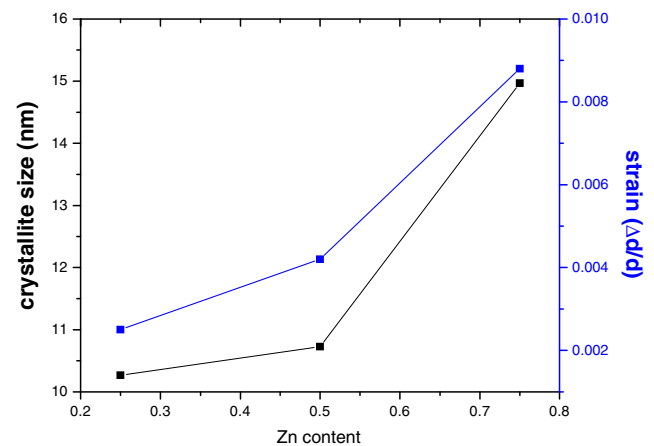
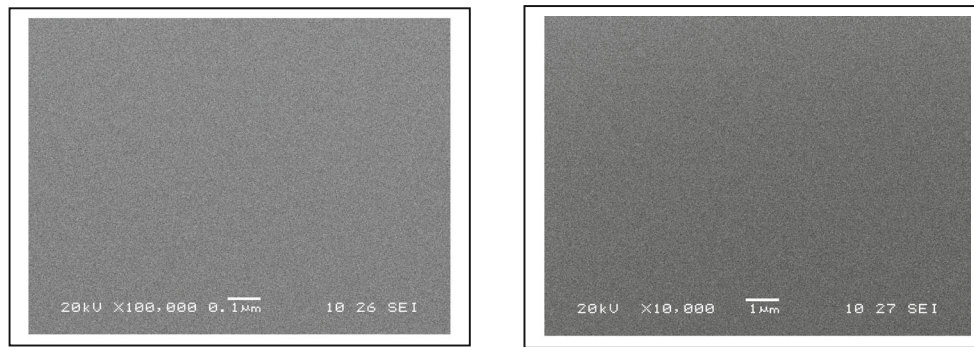
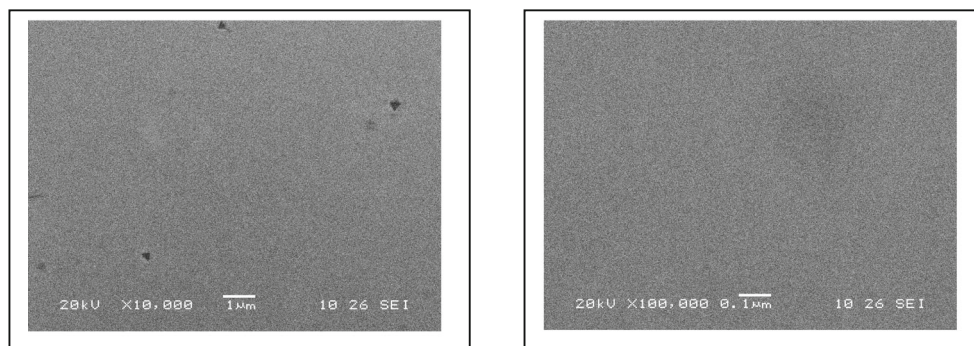


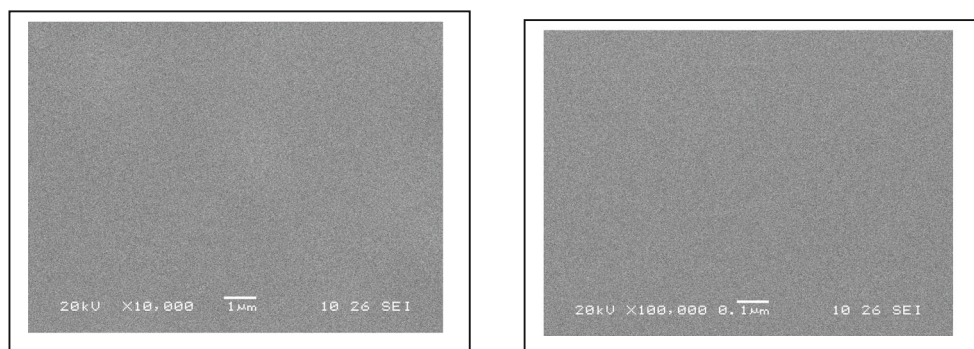
Fig. 4 Variation of crystallite size and strain of $\text{Ni}_{1-x}\text{Zn}_x\text{Fe}_2\text{O}_4$ ($x = 0.25, 0.5, 0.75$) ferrite thin films



(a) SEM image of $\text{Ni}_{0.75}\text{Zn}_{0.25}\text{Fe}_{204}$ ferrite thin films



(b) SEM image of $\text{Ni}_{0.50}\text{Zn}_{0.50}\text{Fe}_{204}$ ferrite thin films.



(c) SEM image of $\text{Ni}_{0.25}\text{Zn}_{0.75}\text{Fe}_{204}$ ferrite thin films.

Fig. 5 **a** SEM image of $\text{Ni}_{0.75}\text{Zn}_{0.25}\text{Fe}_{204}$ ferrite thin films. **b** SEM image of $\text{Ni}_{0.50}\text{Zn}_{0.50}\text{Fe}_{204}$ ferrite thin films. **c** SEM image of $\text{Ni}_{0.25}\text{Zn}_{0.75}\text{Fe}_{204}$ ferrite films

content. Weak absorption hump prominently observed for $x = 0.25$ sample at 630 nm is attributed to $d-d$ transition in Fe^{3+} ion in an octahedral symmetry. Optical absorption bands observed for spinel ferrites are attributed to intra atomic $d-d$ transitions in the Fe^{3+} cations and inter atomic $\text{Fe}^{3+}-\text{O}^{2-}$ transitions between oxygen atomic 2p-orbitals and iron atomic 3d (t_{2g})-orbitals. Zinc inter atomic $\text{Zn}^{2+}-\text{O}^{2-}$ transitions takes place in the UV region which forms Zn^{2+} ion with a completely full 3d sub-shell [31]. Similar to that of iron, in case of nickel different valence ions with

intra-atomic $d-d$ transitions takes place in the NIR region [32]. Figure 7 shows the optical transmission spectra of $\text{Ni}_{1-x}\text{Zn}_x\text{Fe}_2\text{O}_4$ ($x = 0.25, 0.5, 0.75$) ferrite films. It is seen from the Fig. 7 that transmittance increases with increase in wavelength in all cases. In all the cases, the maximum transmittance is about $\sim 90\%$ at wavelength above 700–800 nm. It is seen that as the Zn content increases the transmittance goes on increasing in the range 400–750 nm. The high transparency is associated with a good structural homogeneity and crystallinity.

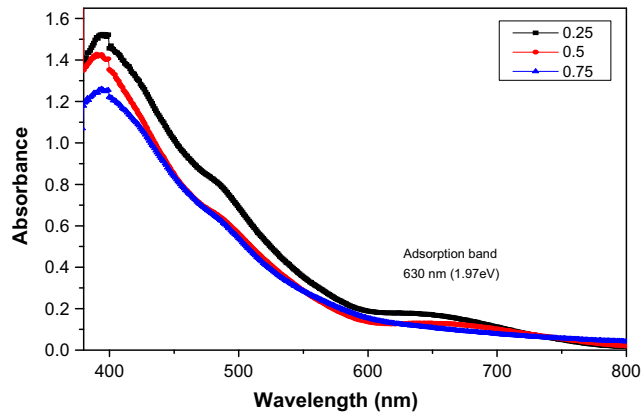


Fig. 6 Absorbance spectra of $\text{Ni}_{1-x}\text{Zn}_x\text{Fe}_2\text{O}_4$ ($x = 0.25, 0.5, 0.75$) ferrite thin films

In high absorption region, optical band gap can be calculated from the relation (5) [33]

$$\alpha = \frac{B (h\nu - E_g)^n}{h\nu} \quad (5)$$

where B is the constant depending on the transition probability. E_g is the optical band gap, $h\nu$ is the photon energy, and n is the constant equal to 1/2 or 2 for allowed direct or indirect transition and 3/2 or 3 for forbidden direct or indirect transition probability.

The plot of $(\text{Absorbance})^2$ against $h\nu$ are plotted (Fig. 8) for estimating the value of direct band gap energy of Ni-Zn ferrite films by extrapolating curves to zero adsorption coefficient. The estimated direct optical band gap energies of $\text{Ni}_{1-x}\text{Zn}_x\text{Fe}_2\text{O}_4$ ($x = 0.25, 0.5, 0.75$) ferrite films are found to be 2.24, 2.49, 2.54 eV, respectively. The value of band gap increases as Zn content increases. There is

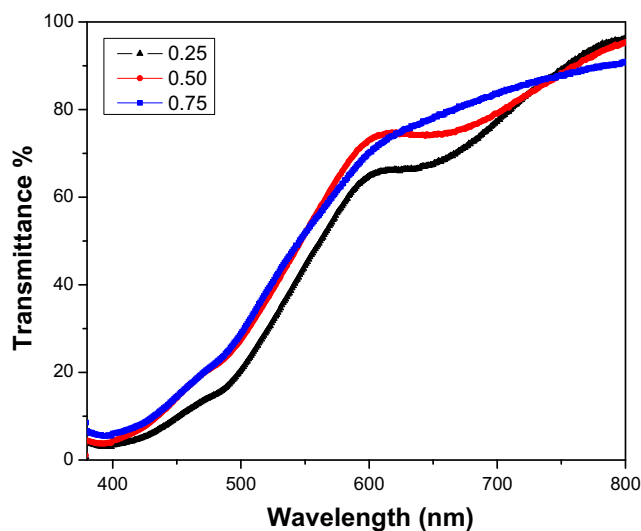


Fig. 7 Transmittance spectra of $\text{Ni}_{1-x}\text{Zn}_x\text{Fe}_2\text{O}_4$ ($x = 0.25, 0.5, 0.75$) ferrite thin films

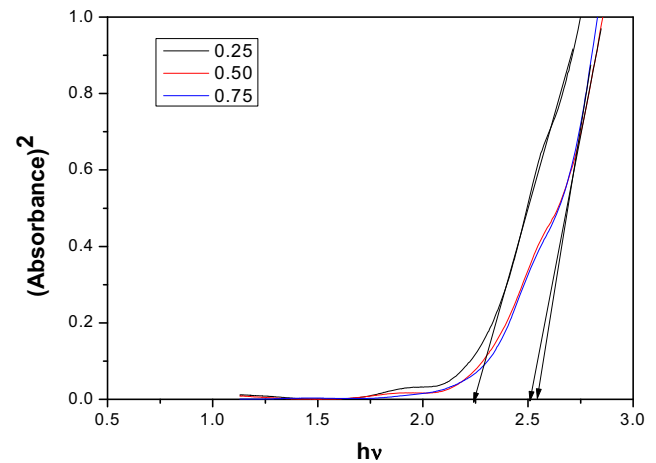


Fig. 8 Plot of $(\text{absorbance})^2$ versus photon energy ($h\nu$) obtained for $\text{Ni}_{1-x}\text{Zn}_x\text{Fe}_2\text{O}_4$ ($x = 0.25, 0.5, 0.75$) ferrite thin films

blue shift ($E_g = 2.24, 2.49, 2.54$) for all Zn-doped samples ($x = 0.25, 0.50, 0.75$), indicating that they may have visible-light photo activity. As there is increase in the optical band gap energy with the increase in the particle size, this is contrast to the normal quantum confinement properties. M. Sundararajan et al. [34] observed that doping of Zn^{2+} to CoFe_2O_4 results into decreased band gap with increase in Zn content. The band gap value of the films is influenced by the various factors such as lattice strain, structural parameters, crystallite size, and presence of impurities.

The complex refractive index function describes the performance and characteristics of the optical properties of solid materials. The complex refractive index function can be expressed by [35].

$$n^* = n - ik \quad (6)$$

The real part of (6) is the refractive index n and the imaginary part is extinction coefficient k . The refractive index (n) and extinction coefficient (k) was determined using the relation given as follows:

$$R = \frac{(n-1)^2}{(n+1)^2} \text{ and } k = \frac{\alpha\lambda}{4\pi} \quad (7)$$

where R is reflectance and n is refractive index. The evaluation of refractive indices of optical materials is of considerable importance for applications in integrated optical devices such as switches, filters, and modulators, where the refractive index of a material is the key parameter for device design. Figure 9 shows the variation of refractive index (n) of $\text{Ni}_{1-x}\text{Zn}_x\text{Fe}_2\text{O}_4$ ($x = 0.25, 0.5, 0.75$) ferrite films with the wavelength.

Figure 9 shows that the refractive index increases with increase in wavelength up to wavelength ~ 540 nm and then decreases with further increases in wavelength. It is also

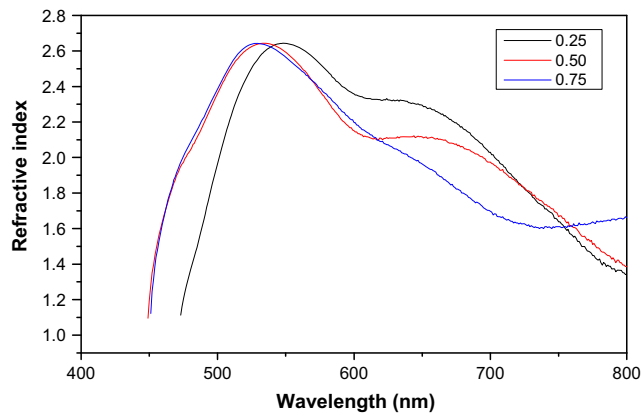


Fig. 9 Variation of refractive index of $\text{Ni}_{1-x}\text{Zn}_x\text{Fe}_2\text{O}_4$ ($x = 0.25, 0.5, 0.75$) ferrite thin films

observed that as Zn content increases, shape of the curves remains same. As we increase Zn content, maximum refractive index is shifted towards lower wavelengths. Variation in refractive index is due to the change in reflectance of the film. For ($x = 0.75$) Zn content after ~ 730 nm wavelength, the refractive index increases. Due to the high refractive index of Ni-Zn ferrite films, it can be used as one of the layers in multilayer antireflection coatings, or as the outer layer of a dielectric pair coating to boost the reflectance of metals.

Figure 10 shows the variation of extinction coefficient (k) of $\text{Ni}_{1-x}\text{Zn}_x\text{Fe}_2\text{O}_4$ ($x = 0.25, 0.5, 0.75$) ferrite films with the wavelength. Figure 10 shows that extinction coefficient of films decreases with increases in wavelength. As Zn content increases, the value of extinction coefficient decreases. The decrease in extinction coefficient with an increase in wavelength in the range 400–800 nm shows that the fraction of light lost due to scattering and absorbance decreases in this region.

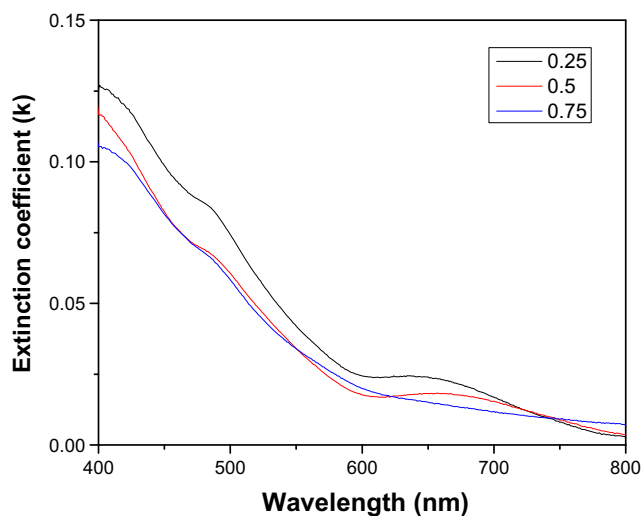


Fig. 10 Variation of extinction coefficient of $\text{Ni}_{1-x}\text{Zn}_x\text{Fe}_2\text{O}_4$ ($x = 0.25, 0.5, 0.75$) ferrite thin films

The optical response of a material is mainly studied in terms of the optical conductivity (σ) which is given by the relation

$$\sigma = \frac{\alpha nc}{4\pi} \tag{8}$$

where α is the absorption coefficient, c is the velocity of light, and n is the refractive index. It can be seen clearly that the optical conductivity directly depends on the absorption coefficient and the refractive index of the material. Figure 11 shows variation of optical conductivity of $\text{Ni}_{1-x}\text{Zn}_x\text{Fe}_2\text{O}_4$ ($x = 0.25, 0.5, 0.75$) ferrite films with incident photon energy. It is seen from Fig. 11 that as Zn content increases the optical conductivity increases. Optical conductivity increases with photon energy in the range 1.55 to 2.56 eV. Its maximum value is 32.45×10^{11} at 2.56 eV for ($x = 0.75$) Zn content, 10.99×10^{11} at 2.56 eV for ($x = 0.50$) Zn content, 9.54×10^{11} at 2.44 eV for ($x = 0.25$) Zn content. The increase in optical conductivity in the photon energy range 1.55 to 2.56 eV can be attributed to the increase in absorption coefficient in this energy range.

The conductivity is nearly constant up to 2 eV of photon energy; after that, it increases with increase in photon energy which suggests increased absorption of photon by film at higher energy. The conductivity peak of the films increases with increase in Zn content. It can be seen clearly that the optical conductivity directly depends on the absorption coefficient.

3.4 Electrical Resistivity

DC resistivity of $\text{Ni}_{1-x}\text{Zn}_x\text{Fe}_2\text{O}_4$ ($x = 0.25, 0.5, 0.75$) ferrite was studied by using two probe method in the

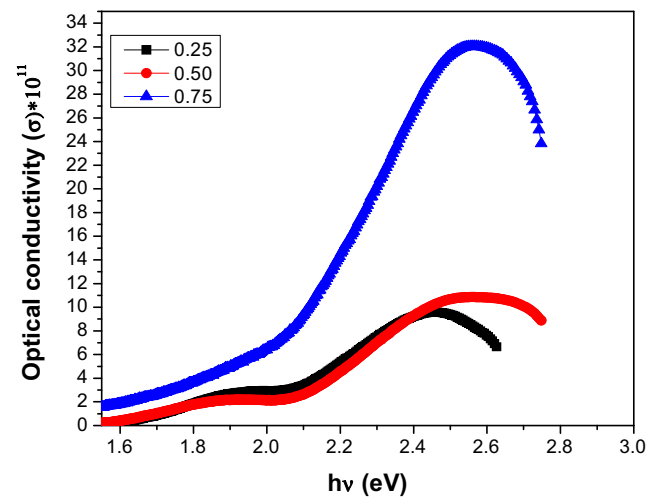


Fig. 11 Variation of optical conductivity with incident photon energy for $\text{Ni}_{1-x}\text{Zn}_x\text{Fe}_2\text{O}_4$ ($x = 0.25, 0.5, 0.75$) ferrite thin films

temperature range 300 to 600 K. The DC resistivity was calculated using relation,

$$\rho = \frac{RA}{l} \quad (9)$$

where R is the DC resistance, A is the area of cross section, and l is the length.

The variation of $\log \rho$ against $1000/T$ for $\text{Ni}_{1-x}\text{Zn}_x\text{Fe}_2\text{O}_4$ ($x = 0.25, 0.5, 0.75$) ferrite films are presented in Fig. 12. The electrical resistivity of the films at room temperature are found to be of the order of $10^6 \Omega \text{ cm}$. From Fig. 12, it is observed that the electrical resistivity of all the films decreases with increasing temperature, suggesting the semiconducting nature of the samples.

The decrease in DC resistivity of ferrites with increasing temperature is attributed to the increase in the drift mobility of electric carriers which are thermally activated with increasing temperature. Also, the conduction in ferrites is due to hopping of electrons between the Fe^{2+} and Fe^{3+} ions at elevated temperature [36–38]. The number of such ion pairs depends on annealing condition and amount of reduction of Fe^{2+} to Fe^{3+} at elevated temperature. The resistivity of ferrite is controlled by Fe^{2+} concentration on B site.

It is also observed that the resistivity of samples decreases with increase in Zn^{2+} content in the sample. Decrease in resistivity on increasing Zn may be due to the fact that Zn ions prefer the occupation of tetrahedral (A) sites and Ni ions prefer the occupation of octahedral (B) sites, while Fe ions partially occupy the A and B sites. On increasing Zn substitution (at A sites), Ni ion concentration (at B sites) will decrease, and hence, resistivity decreases on increasing Zn ion substitution. Therefore, ρ decreases

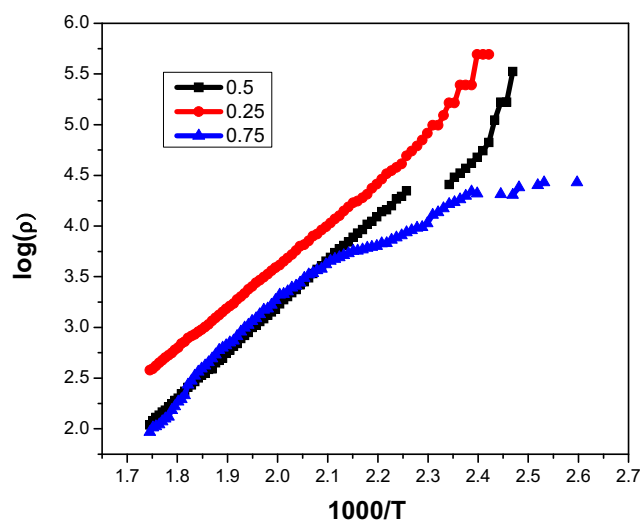


Fig. 12 Variation of $\log \rho$ versus $1000/T$ for $\text{Ni}_{1-x}\text{Zn}_x\text{Fe}_2\text{O}_4$ ($x = 0.25, 0.5, 0.75$) ferrite thin films

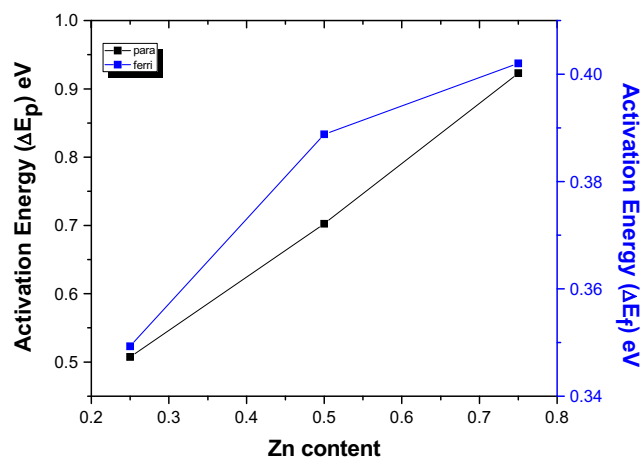


Fig. 13 Variation of activation energy (ΔE_p) and (ΔE_f) for $\text{Ni}_{1-x}\text{Zn}_x\text{Fe}_2\text{O}_4$ ($x = 0.25, 0.5, 0.75$) ferrite thin films

by increasing Zn contents. Similar trend but with different magnitude of resistivity have been reported by Ghazanfar et al. [39].

The activation energies in ferrimagnetic and paramagnetic region of all the films were calculated from the resistivity plots. The dependence of activation energy in ferromagnetic region (ΔE_f) and paramagnetic region (ΔE_p) with Zn content in Ni-Zn ferrite films is shown in Fig. 13 and presented in Table 2. Activation energy is found to be greater in paramagnetic region than ferromagnetic region for all the samples. The value of activation energy increases as the Zn concentration is increased from 0.25 to 0.75. The increase in activation energy may be attributed to the creation of small number of oxygen vacancies [40]. It may also be justified due to the decrease in resistivity with the increase in Zn concentration because activation energy behaves in the same way as that of dc electrical resistivity [41].

3.5 Magnetic Properties

The magnetic properties of the synthesized Ni-Zn ferrite films are analyzed using a vibrating sample magnetometer (VSM) at room temperature. Figure 14 shows the M–H loops of $\text{Ni}_{1-x}\text{Zn}_x\text{Fe}_2\text{O}_4$ ($x = 0.25, 0.5, 0.75$) ferrite films. Ni-Zn ferrite is a soft magnetic material when Ni^{2+} in

Table 2 Activation energy in ferrimagnetic (ΔE_f) and paramagnetic (ΔE_p) region obtained for $\text{Ni}_{1-x}\text{Zn}_x\text{Fe}_2\text{O}_4$ ($x = 0.25, 0.5, 0.75$) ferrite thin films

Zn content	ΔE_f (eV)	ΔE_p (eV)
0.25	0.34	0.50
0.5	0.38	0.70
0.75	0.40	0.92

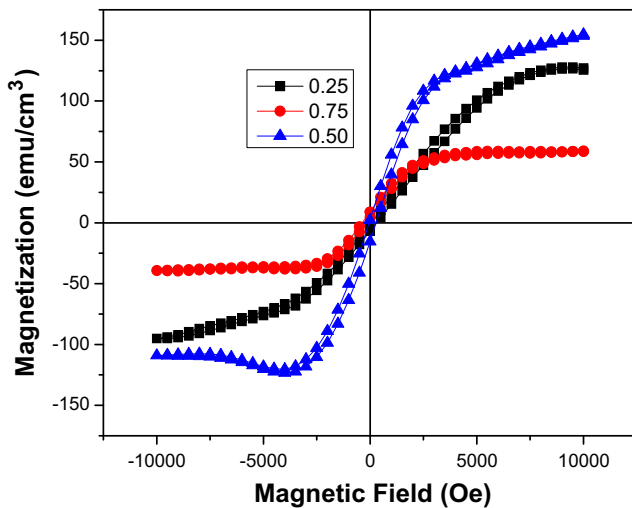


Fig. 14 Magnetic hysteresis loop for $\text{Ni}_{1-x}\text{Zn}_x\text{Fe}_2\text{O}_4$ ($x = 0, 0.25, 0.5, 0.75$) ferrite thin films

NiFe_2O_4 is replaced by Zn^{2+} ions, there is a severe change in the magnetic properties like saturation magnetization (M_s), remanent magnetization (M_r), and coercivity (H_c) are shown in Fig. 14. It is observed that M_s of $\text{Ni}_{1-x}\text{Zn}_x\text{Fe}_2\text{O}_4$ ($x = 0.25, 0.5, 0.75$) films gradually increased with the increase of Zn^{2+} content until $x = 0.5$ and decreased for x larger than 0.5, which is in agreement with literature [42–44]. Also, it is noted that values of M_s , M_r , and H_c of the Ni-Zn Ferrite films are quite smaller than the bulk specimens. Small value of coercive force is observed with negligible retentivity, which indicates the ferrimagnetic nature of the material [45, 46]. The observed results are due to the fact that nickel ferrites possesses inverse spinel structure with all the Ni^{2+} ions in B sites and the Fe^{3+} ions are evenly divided between the A and B sites. The magnetic moments of the Fe^{3+} ions in the A and B sites cancel each other and the net moment is only due to the Ni^{2+} ions. Zinc ferrites have the normal structure with Zn^{2+} ions of zero magnetic moment in the A sites producing no AB interaction. The weakest BB interaction play the role and the Fe^{3+} ions on B sites have antiparallel moments providing no net moment [47].

According to Neel's theory [48], the magnetic moments of cations at the A or B sites are aligned parallel to their neighbors and between A and B sites the arrangement is antiparallel. The magnetic moments are the sum of magnetic moments of cations of A and B sites. Replacement of Ni^{2+} by Zn^{2+} means the introduction of non-magnetic Zn^{2+} ions into A sites and Fe^{3+} ions into B sites, leading to an increase of the net magnetic moments. However, with the continuous doping of Zn ions, the BB interaction gradually take the dominant position instead of the A–B interaction, leading to a drop of the saturation magnetization.

4 Conclusions

Sol–gel spin coating method has been used to obtain $\text{Ni}_{1-x}\text{Zn}_x\text{Fe}_2\text{O}_4$ ($x = 0.25, 0.5, 0.75$) ferrite films. This method allows the formation of films at relatively low temperature. Method provides films with spinel structure and nanometric particles. XRD analysis confirmed the formation of spinel phase $\text{Ni}_{1-x}\text{Zn}_x\text{Fe}_2\text{O}_4$ ($x = 0.25, 0.5, 0.75$) ferrite. The crystallite size was calculated from the XRD peaks confirmed in the range of 10.27 to 14.97 nm in size. The films deposited exhibits smooth and uniform surface, uniform thickness. The grains are regular in shape and particles are found as agglomerated. As Zn content increases, the absorbance goes on decreasing and transmittance goes on increasing in the range 400–750 nm. The high transparency is associated with a good structural homogeneity and crystallinity. Weak absorption hump prominently observed for $x = 0.25$ sample at 630 nm is attributed to $d-d$ transition in Fe^{3+} ion in an octahedral symmetry. Optical band gap of the Ni-Zn samples was found to be shift to higher energy with increase in Zn content in the range of 2.24 to 2.54 eV. The optical band gap of the film increases and increase in crystallite size, this is contrast to the normal quantum confinement properties. As Zn content increases, maximum refractive index is shifted towards lower wavelengths. Variation in refractive index is due to the change in reflectance of the film. Due to the high refractive index of Ni-Zn ferrite films, it can be used as one of the layers in multilayer antireflection coatings or as the outer layer of a dielectric pair coating to boost the reflectance of metals. The decrease in extinction coefficient with an increase in wavelength in the range 400–800 nm shows that the fraction of light lost due to scattering and absorbance decreases in this region. Significant increase in optical conductivity has been noted for the sample maximum Zn content, i.e., for $x = 0.75$ sample. The conductivity is nearly constant up to 2 eV of photon energy; after that, it increases with increase in photon energy which suggests increased absorption of photon by film at higher energy. It can be seen clearly that the optical conductivity directly depends on the absorption coefficient.

Electrical conductivity of the films increasing with temperature indicates semiconducting nature as expected. Activation energy is found to be greater in paramagnetic region than ferromagnetic region for all the samples. The VSM results revealed that saturation magnetization M_s of films gradually increases up to $x = 0.5$ and decreases for x larger than 0.5. Small value of coercive force is observed with negligible retentivity, which indicates the ferrimagnetic nature of the material.

Acknowledgments The authors are thankful to University of Grants Commission (UGC) WRO Pune for the financial support.

References

- Manikandan, A., Sridhar, R., Arul Antony, S., Ramakrishna, S.: A simple aloe vera plant-extracted microwave and conventional combustion synthesis: morphological, optical, magnetic and catalytic properties of CoFe_2O_4 nanostructures. *J. Mol. Struct.* **1076**, 188–200 (2016)
- Amir, M., Geleri, M., Guner, S., Baykal, A., Sozeri, H.: Magneto optical properties of $\text{FeB}_x\text{Fe}_{2-x}\text{O}_4$ nanoparticles. *J. Inorg. Organomet. Polym.* **25**, 1111–1119 (2015)
- Manikandan, A., Saravanan, A., Arul, A.S., Bououdina, M.: One-pot low temperature synthesis and characterization studies of nanocrystalline $\alpha\text{-Fe}_2\text{O}_3$ based dye sensitized solar cells. *J. Nanosci. Nanotech* **15**, 4358–4366 (2015)
- Manikandan, A., Durka, M., Arul, A.S.: One-pot flash combustion synthesis, structural, morphological and opto-magnetic properties of spinel $\text{Mn}_x\text{Co}_{1-x}\text{Al}_2\text{O}_4$ ($x = 0, 0.3, \text{ and } 0.5$) Nanocatalysts. *J. Supercond. Nov. Magn.* **28**, 209–218 (2015)
- Amir, M., Baykal, A., Güner, S., Sertkol, M., Sözeri, H.: M.: Toprak Synthesis and characterization of $\text{Co}_x\text{Zn}_{1-x}\text{AlFeO}_4$ nanoparticles. *J. Inorg. Organomet Polym* **25**, 747–754 (2015)
- Manikandan, A., Durka, M., Arul, A.S.: A novel synthesis, structural, morphological, and opto-magnetic characterizations of magnetically separable spinel $\text{Co}_x\text{Mn}_{1-x}\text{Fe}_2\text{O}_4$ ($0 \leq x \leq 1$) Nano-catalysts. *J. Supercond. Nov. Magn.* **27**, 2841–2857 (2014)
- Sugimoto, M.: The past, present, and future of ferrites. *J. Am. Ceram. Soc.* **82**(2), 269–280 (1999)
- Sun, S., Murray, C.B., Weller, D., Folks, L., Moser, A.: Monodisperse FePt nanoparticles and ferromagnetic FePt nanocrystal superlattices. *Science* **287**, 1989–1992 (2000)
- Liu, Y.-L., Liu, Z.-M., Yang, Y., Yang, H.-F., Shen, G.-L., Yu, R.-Q.: Simple synthesis of MgFe_2O_4 nanoparticles as gas sensing materials. *Sens. Actuators B* **107**, 00–604 (2005)
- Dom, R., Subasri, R., Radha, K., Borse, P.H.: Synthesis of solar active nanocrystalline ferrite, MFe_2O_4 (M: Ca, Zn, Mg) photocatalyst by microwave irradiation. *Solid State Commun* **151**, 470–473 (2011)
- Zi, Z., Lei, H., Zhu, X., Wang, B., Zhang, S., Zhu, X., Song, W., Sun, Y.: Influence of annealing temperature on surface morphology and magnetic properties of $\text{Ni}_{0.7}\text{Zn}_{0.3}\text{Fe}_2\text{O}_4$ ferrite thin films. *Mater. Sci. Eng. B* **167**, 70–73 (2010)
- Zahi, S., Hashim, M., Daud, A.R.: Synthesis, magnetic properties and microstructure of Ni-Zn ferrite by sol-gel technique. *J. Magn. Magn. Mater.* **308**, 177 (2007)
- Shimada, Y., Matsushita, N., Abe, M., Kondo, K., Chiba, T., Yoshida, S.: Study on initial permeability of Ni-Zn ferrite films prepared by the spin spray method. *J. Magn. Magn. Mater.* **278**, 256 (2004)
- Guo, D., Fan, X., Chai, G., Jiang, C., Li, X., Xue, D.: Structural and magnetic properties of NiZn ferrite films with high saturation magnetization deposited by magnetron sputtering. *Appl. Surf. Sci.* **256**, 2319–2322 (2010)
- Ravinder, D., Vijay Kumar, K., Ramana Reddy, A.V.: Preparation and magnetic properties of Ni-Zn ferrite thin films. *Mater. Lett.* **57**, 4162–4164 (2003)
- Gupta, N., Verma, A., Kashyap, S.C., Dube, D.C.: Dielectric behavior of spin-deposited nanocrystalline nickel-zinc ferrite thin films processed by citrate-route. *Solid State Commun.* **134**, 689–694 (2005)
- Beji, Z., Smiri, L.S., Vaulay, M.-J., Herbst, F., Ammar, S., Fiévet, F.: Nanocrystalline $\text{Ni}_{0.8}\text{Zn}_{0.2}\text{Fe}_2\text{O}_4$ films prepared by spray deposition from polyol-mediated sol: microstructural and magnetic characterization. *Thin Solid Films* **518**, 2592–2598 (2010)
- Kashif, M., Hasim, U., Ali, M.E., Ali, S.M.U., Rusop, M., Ibpoto, Z.H., Willander, M.: Effect of different seed solutions on the morphology and electrooptical properties of ZnO nanorods. *J. Nanomater.* **2012**, 106 (2012). doi:10.1155/2012/452407
- Khan, J.A., Qasim, M., Singh, B.R., Singh, S., Shoeb, M., Khan, W., Das, D., Naqvi, A.H.: Synthesis and characterization of structural, optical, thermal and dielectric properties of polyaniline/ CoFe_2O_4 nanocomposites with special reference to photocatalytic activity. *Spectrochim. Acta A Mol. Biomol. Spectrosc.* **109**, 313–321 (2013)
- Qasim, M., Asghar, K., Singh, B.R., Prathapani, S., Khan, W., Naqvi, A.H., Das, D.: Magnetically recyclable $\text{Ni}_{0.5}\text{Zn}_{0.5}\text{Fe}_2\text{O}_4/\text{Zn}_{0.95}\text{Ni}_{0.05}\text{O}$ nano-photocatalyst: structural, optical, magnetic and photocatalytic properties. *Spectrochim. Acta A Mol. Biomol. Spectrosc.* **137**, 1348–1356 (2015)
- Herve, P., Sadou, A.: Determination of the complex index of refractory metals at high temperatures: application to the determination of thermo-optical properties. *Infrared Phys. Technol.* **51**, 249–255 (2008)
- Mechiakh, R., Bensaha, R.: Analysis of optical and structural properties of sol-gel TiO_2 , thin films Moroccan. *J. Condens. Matter* **7**(1), 54–57 (2006)
- Gasanly, N.M.: Temperature-tuned band gap energy and oscillator parameters of $\text{Tl}_2\text{InGaSe}_4$ semiconducting layered single crystals. *Cryst. Res. Technol.* **44**(3), 322–326 (2009)
- Pawar, C.S., Gujar, M.P., Mathe, V.L.: Synthesis and characterization of nano crystalline nickel zinc ferrite for chlorine gas sensor at room temperature. *AIP Conf. Proc.* **1665**, 050060 (2015). doi:10.1063/1.4917701
- Sutka, A., Lagzdina, S., Mezinskis, G., Pludons, A., Vitina, I., Timma, L.: A comparative study of $\text{Ni}_{0.7}\text{Zn}_{0.3}\text{Fe}_2\text{O}_4$ obtained by sol-gel auto-combustion and flash combustion methods. *IOP Conf. Series: Materials Science and Engineering* **25**, 012019 (2011). doi:10.1088/1757-899X/25/1/012019
- Gul, I.H., Amin, F., Abbasi, A.Z., Anis-ur-Rehman, M., Maqsood, A.: Physical and magnetic characterization of co-precipitated nanosize Co-Ni ferrites. *Scripta Mater.* **56**, 497–500 (2007)
- Hamedoun, M., Benyoussef, A., Bousmina, M.: Magnetic properties and phase diagram of $\text{Zn}_x\text{Ni}_{1-x}\text{Fe}_2\text{O}_4$: high-temperature series expansions. *J. Magn. Magn. Mater.* **322**, 3227–3235 (2010)
- Gul, I.H., Ahmed, W., Maqsood, A.: Electrical and magnetic characterization of nanocrystalline Ni-Zn ferrite synthesis by co-precipitation route. *J. Magn. Magn. Mater.* **320**, 270–275 (2008)
- Riaz, S., Naseem, S.: Effect of reaction temperature and time on the structural properties of $\text{Cu}(\text{In}, \text{Ga})\text{Se}_2$ thin films deposited by sequential elemental layer technique. *J. Mater. Sci. Technol.* **23**, 499–503 (2007)
- Cullity, B.D.: Elements of X-ray Diffraction. Addison-Wesley, USA (1956)
- Virden, A.E., O'Grady, K.: The temperature dependence of magnetization in ferrofluids. *J. Appl. Phys.* **99**, 08S106 (2006). doi:10.1063/1.2172892
- Billmeyer Jr., F.W., Saltzman, M.: Wiley, New York (1981)
- Mott, N.F., Gurney, R.W.: Electronic Processes in Ionic Crystals (1940)
- Sundararajan, M., John Kennedy, L., Judith Vijaya, J., Aruldoss, U.: Microwave combustion synthesis of $\text{Co}_{1-x}\text{Zn}_x\text{Fe}_2\text{O}_4$ ($0 \leq x \leq 0.5$): structural, magnetic, optical and vibrational spectroscopic studies. *Spectrochim. Acta A Mol. Biomol. Spectrosc.* **140**, 421–430 (2015)
- Walton, A.K., Moss, T.S.: Determination of refractive index and correction to effective electron Mass in PbTe and PbSe. *Proc. Phys. Soc.* **81**(3), 509–513 (1963)
- Gadkari, A.B., Shinde, T.J., Vasambekar, P.N.: Electrical and humidity sensing study of Nanocrystallite Mg-Cd Ferrites. *Sens. Trans. J.* **137**(2), 145–154 (2012)

37. Manjula, R.: Ferrites, Material Science and Technology, 25–26 (1990)
38. Vishwanathan, B., Murthy, V.R.K.: Ferrites, and Material Science and Technology. Norosa Pub. House, New Delhi (India) (1990)
39. Ghazanfar, U., Siddiqi, S.A., Abbas, G.: Study of room temperature DC resistivity in comparison with activation energy and drift mobility of NiZn ferrites. *Mater. Sci. Eng. B* **118**, 132–134 (2005)
40. Islam, M.U., Ahmad, I., Abbas, T., Chaudhry, M.A., Nazmeen, R.: Advanced materials. In: Proceedings of the 6th International Symposium, p. 155 (1999)
41. El-Shabasy, M.: DC electrical properties of ZnNi ferrites. *J. Magn. Magn. Mater.* **172**, 188–192 (1997)
42. Costaa, A.C.F.M., Tortellab, E., Morellib, M.R., Kiminami, R.H.G.A.: Synthesis, microstructure and magnetic properties of Ni-Zn ferrites. *J. Magn. Magn. Mater.* **256**, 174–182 (2003)
43. Li, Y., Li, Q., Wen, M., Zhang, Y., Zhai, Y., Xie, Z., Xu, F., Wei, S.: Magnetic properties and local structure studies of Zn doped ferrites. *J. Electron Spectrosc. Relat. Phenom.* **160**, 1–6 (2007)
44. Rana, M.U., Abbas, T.: The effect of Zn substitution on microstructure and magnetic properties of $\text{Cu}_{1-x}\text{Zn}_x\text{Fe}_2\text{O}_4$ ferrite. *J. Magn. Magn. Mater.* **246**, 110–114 (2002)
45. Singh, K., Ohlan, A., Kotnala, R.K., Bakhshi, A.K., Dhawan, S.K.: Dielectric and magnetic properties of conducting ferromagnetic composite of polyaniline with $\gamma\text{-Fe}_2\text{O}_3$ nanoparticles. *Mater. Chem. Phys.* **112**, 651–658 (2008)
46. Xiao, H.-M., Liu, X.-M., Fu, S.-Y.: Synthesis, magnetic and microwave absorbing properties of core-shell structured $\text{MnFe}_2\text{O}_4/\text{TiO}_2$ nanocomposites. *Compos. Sci. Technol.* **66**, 2003–2008 (2006)
47. Cullity, B.D.: Introduction to Magnetic Materials. Addison Wesley Publishing Company (1972)
48. Duque, J.G.S., Souza, E.A., Meneses, C.T., Kubota, L.: Magnetic properties of NiFe_2O_4 nanoparticles produced by a new chemical method. *Phys. B Condens. Matter* **398**, 287–290 (2007)